Glioblastoma on a microfluidic chip: Generating pseudopalisades and enhancing aggressiveness through blood vessel obstruction events

Jose M. Ayuso[123], Rosa Monge[123], Alicia Martínez-González[4], María Virumbrales-Muñoz[123], Guillermo A. Llamazares[123], Javier Berganzo[5], Aurelio Hernández-Laín[6], Jorge Santolaria[7], Manuel Doblaré[123], Christopher Hubert[8], Jeremy N. Rich[8], Pilar Sánchez-Gómez[9], Víctor M. Pérez-García[4], Ignacio Ochoa[123*], Luis J. Fernández[123*].

1 Group of Structural Mechanics and Materials Modelling (GEMM). Centro Investigación Biomédica en Red. Bioingenieria, biomateriales y nanomedicina (CIBER-BBN), Spain.

2 Aragón Institute of Engineering Research (I3A), University of Zaragoza, Spain.

3 Aragon Institute of Biomedical Research, Instituto de Salud Carlos III, Spain.

4 Institute of Applied Mathematics in Science and Engineering, Castilla-La Mancha University, Spain.

5 MEMS/MST Department, Ikerlan S. Coop., Mondragón, Spain.

6 Department of Pathology (Neuropathology), Hospital Universitario 12 de Octubre Research Institute, Madrid, Spain.

7 Department of Design and Manufacturing Engineering, University of Zaragoza, Spain.

8 Department of Stem Cell Biology and Regenerative Medicine, Lerner Research Institute, Cleveland Clinic, Cleveland, OH 44195

9 Neuro-oncology unit. Health institute Carlos III-UFIEC, Spain.

* These authors equally coordinate this project.

Running title: Glioblastoma pseudopalisades on a chip

Corresponding author: Luis José Fernández. Mailing address: Mariano Esquillor, Zaragoza, Zaragoza, Spain, 50018. Phone: 876555467. Fax: 976762043. E-Mail: luisf@unizar.es

Funding: Projects (dpi2011-28262-c04-01), (MTM2012-31073), (bes-2012-059940)"; and the "Junta de Comunidades de Castilla-La Mancha/FEDER" (PEII-2014-031-P). "Ministerio de Economía y Competitividad, Fondo de Investigación Sanitaria" (PI12/00775 to P.S.G., PI13/01258 to A.H.L); "Ministerio de Economía y Competitividad, Red Temática de Investigación Cooperativa en Cancer" (RD12/0036/0027 to P.S.G. and A.H.L.) and by The National Institutes of Health (CA189647 to C.G.H., CA154130, CA171652, CA169117, NS087913, NS089272 to J.N.R); Research Programs Committees of Cleveland Clinic (J.N.R), and James S. McDonnell Foundation (J.N.R).

Conflict of interests: All the authors declare no competing interests.

Word count: 6433

ABSTRACT

Background: Glioblastoma (GBM) is one of the most lethal tumor types. Hypercellular regions, named pseudopalisades, are characteristic in these tumors and have been hypothesized to be waves of migrating glioblastoma cells. These “waves” of cells are thought to be induced by oxygen and nutrient depletion caused by tumor-induced blood vessel occlusion. Although the universal presence of these structures in GBM tumors suggest that they may play an instrumental role in GBM spreading and invasion, the recreation of these structures in vitro has remained challenging.

Methods: Here we present a new microfluidic model of GBM that mimics the dynamics of pseudopalisade formation. To do this, we embedded U-251 MG cells within a collagen hydrogel in a custom designed microfluidic device. By controlling the medium flow through lateral microchannels, we can mimic and control blood vessel obstruction events associated with this disease.

Results: Through the use of this new system, we show that nutrient and oxygen starvation triggers a strong migratory process leading to pseudopalisade generation in vitro. These results validate the hypothesis of pseudopalisade formation and show an excellent agreement with a systems-biology model based on hypoxia-driven phenomenon.

Conclusions: This paper shows the potential of microfluidic devices as advanced artificial systems capable of modeling in vivo nutrient and oxygen gradients during tumor evolution.

Keywords: Glioblastoma, Microfluidics, Pseudopalisades, SU-8, Migration

INTRODUCTION

Glioblastoma, also named grade IV astrocytoma, is the most common and lethal malignant primary brain tumor. Patients receiving the standard-of-care based on local radiotherapy and concomitant chemotherapy have a median survival of 14 months[1]. Despite the efforts of the research community, new treatments to tackle the disease are still far from the clinic. GBM tumors are highly infiltrating and fast progressing tumors[2] and are characterized by two main histopathological conditions: necrotic foci typically surrounded by areas of high cellularity known as pseudopalisading regions, and microvascular proliferation[2].

The causes of these densely populated pesudopalisades remain poorly understood. Although the high cellularity was initially thought to be due to rapid proliferation of GBM cells, recent histological studies have shown that proliferation in pseudopalisading areas is significantly lower than in adjacent regions[3]. Additionally, in pseudopalisades apoptosis is substantially larger than in neighboring regions[4]. This evidence suggests that pseudopalisades are due to causes other than simply higher proliferation or survival rates. Recent reports have shown that in histological slices from GBM patients more than 50% of pseudopalisades clearly present a central obstructed blood vessel, and microscopic evidence of thrombosis is observed in more than 90% of samples[4-6].

GBM cells express several procoagulant factors which may serve to induce thrombosis[7]. Additional evidence shows that cells in pseudopalisades are hypoxic and overexpress HIF-1α[8]. Although this hypoxic microenvironment leads to microvascular hyperplasia, the associated microcirculation is very inefficient due to parenchymal edema and poor maintenance of the blood brain barrier[9]. As a consequence, the supply of oxygen and nutrients is compromised in the zone surrounding a thrombosis.

GBM evolution is a complex process. It has been proposed that one of the driving forces of glioma aggressiveness is nutrient and oxygen starvation[3,4,10]. First, GBM proliferation and secretion of pro-coagulant signals would causes thrombotic events leading to hypoxia and nutrient depletion. As a consequence, the migration of cells away from a thrombosis and towards nutrients and oxygen enriched regions could create the characteristic GBM pseudopalisades. Eventually, these migrating cells would reach other blood vessels and eventually cause the collapse of these vessels, restarting the process and creating another expanding wave of tumor cells within the brain. This hypothesis proposes that GBM cells are exposed to cyclic starvation which forces their metabolism to switch between a proliferative or migrating phenotype.

Since we cannot take multiple histologic timepoints in vivo, it has not been possible to definitively observe thrombosis-induced migration in real-time and the kinetics of any such migration are not understood. This complex process is not reproducible using standard “in vitro” models because the conventional migration assays are unable to mimic the complex microenvironment described. Recently, microfabrication and microfluidic technologies have arisen, allowing the design and creation of custom high-performance cell culture systems[11]. In this paper we describe the design, fabrication and biological validation of a microfluidic device using SU-8 technology for three-dimensional GBM cell cultures under obstructed conditions. Under these conditions, nutrient starvation leads to a chemotactic process and the formation of a migratory front similar to the pseudopalisades observed in vivo and corresponding to predictive mathematical algorithms. Moreover, our results suggest that the pseudopalisading process stimulates a more aggressive behavior of GBM cells. This novel technique could help us to understand the mechanism of pseudopalisade formation and to suggest novel therapeutic targets to avoid tumor progression. These microfluidic devices represent an extremely useful platform to evaluate cellular behavior and to test

new anticancer agents in a preclinical setting that mimics the complex GBM microenvironment.

METHODS

Microfluidic chip fabrication

Microfluidic devices were fabricated using SU-8 photolithography combined with a SU-8 to SU-8 bonding process. The fabrication process was inspired by previously reported work describing the fabrication of SU-8 microdevices[12,13]. Briefly, several layers of SU-8 were spun onto the Kapton film and different soft bake, UV exposure and post-bake steps were performed[14,15].

Packaging tool fabrication

In order to recreate obstructed conditions (Fig 1A), a regular flow of culture media must be provided to the microdevice through one lateral microchannel whereas the other is sealed (Fig 1B). A dedicated package was designed and fabricated to provide proper housing and hermetic connections to the microdevice inlets and outlets, allowing for automated cellular culture. Final microdevice and packaging tool are showed in Fig. 1C.

Cell culture

C-6 cells were kindly provided by Dr Pešic (University of Belgrade) whereas U-251-MG cells were purchased from ATCC. Both cells were routinely grown in Dulbecco´s modified Eagle´s medium (DMEM) (Lonza BE12-614F) supplemented with 10% v/v fetal bovine serum (Sigma F7524) and penicillin/streptomycin (DE 17-602E) within a TEB-1000 incubator (EBERS Medical Technology). For three-dimensional cultures, all reagents, microdevices included, were placed on ice. Cells were trypsinized and resuspended in a calculated volume of medium (DMEM supplemented with 10 % fetal

bovine serum) to reach the desired concentration of cells in the final hydrogel solution. Using a chilled tip, we prepared a mixture of 24.9 µl of collagen type I 4.01 mg/ml (Corning 354236); 0.62 µl of NaOH 1N (Sigma 655104); 10 µl of DMEM 5X (Sigma D5523), 50 µl of cell solution and 14.5 µl of sterile water. The hydrogel mixture was injected into the device using a micropipette, then a 5 µl droplet was placed on top of the central inlet to prevent hydrogel leakage and evaporation. Afterwards, the microfluidic device was placed into an incubator (37°C and 5% CO_2) for 15 minutes to allow collagen polymerization. For use as a macroscopic control on viability assays, 100 µl of hydrogel mixture was allowed to polymerize on Petri dishes. Medium within microdevices was refreshed once a day. Cell membrane was fluorescently labelled using vibrant DiI (Life Technologies, V-22885) following the supplier instructions.

Cell Viability

Stock solutions of 5 mg/ml Calcein (CAM) (Life technologies C1430) and 2 mg/ml propidium iodide (PI) (Sigma P4170) were prepared following supplier instructions.

To test cell viability within microfluidic devices and in Petri dishes, stock solutions of CAM and PI were diluted to 5 and 4 µg/ml, respectively, in phosphate-buffered saline (PBS) (Lonza BE17-516F). Microdevices and petri controls were washed once with PBS, and then filled with CAM/PI. Confocal images were immediately taken using a Nikon Eclipse Ti microscope equipped with a C1 modular confocal microscope system. Images were collected at different focal planes within each microdevice and Petri control.

Long-term cultures under obstructed conditions.

To mimic the obstructed conditions, cells were embedded into a collagen hydrogel injected within the central microchamber of the microdevices. After 24 hours, the microdevices were loaded into the packaging tool and all inlets were sealed except for

one pair to enable medium perfusion through only one lateral microchannel (Fig. 1D). As a control group, other microdevices were left on the Petri dish and medium was manually refreshed once a day under unrestricted conditions. System evolution was followed and cell viability and distribution was evaluated at different times. Flow profile was characterized using green-fluorescent 0.2 μm diameter spheres (Life Technologies, F8811). Oxygen profile across the microchamber was measured using "Image-it Hypoxia reagent" (Life Technologies, H10498) dissolved in DMSO. Medium supplemented with 10 μM hypoxia reagent was perfused through the system for 24 hours to ensure the reagent reached the microdevice. Continuous oxygen monitoring throughout all the experiment was avoided due to the reagent toxicity. Hypoxia-induced fluorescence was detected using a 488 nm laser coupled with a 650nm long-pass detector in the confocal microscope.

Glucose profile analysis

The presence of a glucose gradient during experiments was studied using a fluorescent glucose (2-NBDG) (Life Technologies N13195) which is imported by the cells in place of glucose. Since 2-NBDG and conventional glucose compete for the cell glucose transporters, cells were cultured within the microdevices in glucose-free DMEM (Thermos Fisher Scientific, 11966-025) supplemented with fetal calf serum, glutamine and antibiotics. This glucose-free medium was supplemented with 2-NBDG at 200 μM and perfused through one lateral microchannel. Time-lapse images were taken for 2 hours every 5 minutes to analyze NBDG penetration across the central microchamber. Long-term experiments with NBDG and absence of conventional glucose were not possible since it may affect cell behavior.

Image analysis

Cell analysis within the central microchamber and Petri controls was performed using automated Fiji software (http://fiji.sc/Fiji). To analyze cell distribution within the central

198 microchamber, only focal planes ranging from 50 μm to 250 μm were used to exclude
199 cells attached directly to the 2D microchamber top and bottom. Selected focal planes
200 were flipped vertically, generating the orthogonal view, which was projected to get the
201 cell distribution across all the microchamber length. In order to analyze cell shape, cell
202 perimeter was drawn manually and ellipse fitted-aspect ratio was calculated as the ratio
203 between the ellipse major and minor axis. Cell directionality was also determined and
204 plotted as a histogram referred to the medium flow direction. At least one hundred cells
205 were analyzed in each region.
206
207 **Immunofluorescence**
208 Samples were fixed for 30 min with 4% paraformaldehyde (VWR J61899-AP),
209 permeabilized using 0,1% Triton-X100 (Sigma T8787) and blocked with 5% BSA
210 (Sigma A2058) in PBS. Samples were then incubated overnight with primary antibody
211 (1/50 in 2,5% BSA and 0,05% Triton X-100, Santacruz anti-Ki-67 sc-23900,), and
212 secondary antibody (1/200) was used under the same conditions. DAPI (Sigma D9542-
213 1MG) staining was performed overnight and after a washing step samples were
214 visualized.
215
216 **Tumor pathology**
217 The human tissues were procured after obtaining the patient written consent and with
218 the approval of the ethics committees of *Hospital Universitario 12 de Octubre*.
219 Hematoxylin-Eosyn (H&E) staining was performed on 5 μm thick sections from paraffin-
220 embedded tumors. Pseudopalisades areas were selected and the nuclear shape in the
221 rear end (close to the necrotic core) or at the front was calculated as previously
222 described. Twenty nuclei were analyzed in each region. Three different samples were
223 analyzed. All methods were carried out in accordance with the approved guidelines.
224
225 **Mathematical modeling**

This model is based on our previous models[10,16] where oxygen coming from straight vessels was the driving force that triggered the normoxic and hypoxic phenotypic changes. To these two dominant phenotypes, based on the go or grow dichotomy[17], we have incorporated a third phenotype accounting for hypoxic cells that arrive to normoxic areas and switch to a more proliferative phenotype. Also, in addition to the diffusive random motion, we have comprised a directional transport term driving the cell's motion towards better oxygenated regions for hypoxic cells that was not present in Refs[10,16].

The mathematical model consists of a set of partial differential equations modelling the interplay of three cellular cancer cell phenotypes, the oxygen distribution and necrosis:

Major assumptions of the Mathematical Model:

1. Hybrid model between *go or grow* and *go and grow* models.
2. Classical logistic space-limited growth for the tumor cell populations.
3. Hypoxic phenotype is more migratory than any other cell phenotype.
4. Oxygen acts as a chemoattractant for hypoxic cells.
5. Malignant cells have the highest proliferation.
6. Homogenous and isotropic oxygen diffusion in the chamber.
7. Oxygen flows from channels to balance the different oxygen pressures.
8. Malignant cells consume more oxygen than any other cell phenotype .

Statistical analysis

Data were analyzed using SPSS software, and statistical significance was set at $p < 0.05$. Results are presented as mean ± standard error. The normal distribution was tested by the Kolmogorov-Smirnov test. For parametric comparison, one way ANOVA with Bonferroni post hoc tests was performed. For nonparametric comparisons, a Kruskal-Wallis test was performed followed by the U-test of Mann-Whitney.

RESULTS

GBM cells are viable in 3-dimensional microchamber culture

The fabricated microdevice possesses a central microchamber to locate the cells embedded within a hydrogel[18-20], mimicking the ECM and allowing migration in three dimensions. On both sides of the microchamber, lateral microchannels are filled with culture medium, allowing nutrient and oxygen diffusion throughout the microchamber, mimicking the function of brain blood vessels.

We first examined microdevice biocompatibility with GBM cells to ensure the material does not affect cell viability. After 7 days in culture, we evaluated U-251 cell viability within microdevices compared to culture dish controls using CAM and propidium iodide (PI). Results showed that cell viability within microdevices was very high (>95%) and more importantly it was similar to culture controls at the same timepoint, validating the use of this microdevice for three dimensional U-251 cell culture (Fig. 1E, F).

Flow profile

Culture medium supplemented with 1% spheres suspension was injected through the lateral microchannel in obstructed conditions to study the flow profile. Fluorescent time-lapse images demonstrated that under obstructed conditions the flow profile was not penetrating into the hydrogel (Supporting Fig. 1A-C), but it was completely parallel to the central microchamber. When an interstitial flow through the central microchamber was externally imposed, the fluorescent spheres invaded the hydrogel in few minutes (Supporting Fig. 1D-F). Therefore, under obstructed conditions the fluid flow is not mechanically affecting the hydrogel or the embedded cells.

GBM cells migrate under obstructed conditions

By controlling medium flow through the lateral microchannels, we can mimic the GBM-associated thrombotic pathophysiological conditions. Under unrestricted conditions, cell distribution within the microchamber was constant throughout the experiment (nine days of culture, Fig. 2A-C). Under obstructed conditions, cell viability continued to be very high (>95%) and we also observed a strong migratory process. After three days of thrombotic conditions, cell migration was barely apparent and only small cell aggregates near the perfused microchannel were visible (Fig. 2D). After six days, migration evolved to the formation of a well-defined front, resembling the in vivo observed pseudopalisades (Fig. 2E). Finally, after nine days this front moved closer to and invaded the perfused microchannel (Fig. 2F). In order to perform a more quantitative and precise analysis, we analyzed the fluorescence intensity across the microchamber. This analysis of cell distribution confirmed that under unrestricted conditions there was no change during the time course (Fig. 2G). On the other hand, after three days under obstructed conditions this distribution showed a moderate increase nearby the perfused lateral microchannel compared to the unrestricted conditions, showing an emerging migratory response (Fig. 2H). After six days, this response increased to a well-defined peak, indicating cells concentrating in this region, creating the characteristic pseudopalisade front and abandoning the occluded rear region. After nine days, the intensity of the pseudopalisade front reached a maximum and was displaced as cells reached the perfused lateral microchannel. This is the first experimental evidence showing the creation of a pseudopalisade front by a migratory wave of GBM cells moving from obstructed to perfused conditions. In order to expand this study using another GBM cell line, C-6 cells were cultured in the microdevice under similar conditions. After 3 days under obstructed conditions, C-6 cells showed an invasion process towards the perfused lateral microchannel (Supporting Fig. 2). Interestingly, C-6 cells exhibited a faster invasion than U-251 MG. Furthermore, a population of dead C-6 cells appeared concentrated nearby the obstructed lateral microchannel. Thereby, C-6 cells seemed to have a faster metabolism compared with

U-251 MG, which led to an accelerated invasion. Longer invasion times using C-6 cells were not analyzed due to a significant hydrogel contraction caused by these cells.

Cell morphology analysis during pseudopalisade formation

Our results suggested that pseudopalisading structures can be created by a migratory response lead by cells located at the rear of the migratory front, near the non-perfused microchannel. We next investigated the morphologic changes in GBM cells during the formation of pseudopalisades. As expected, after 5 days of culture cells under unrestricted conditions appeared identical on either side of the microchamber (Fig. 3A). Conversely, five days after the induction of obstructed conditions cell morphology clearly shifted in the cell population closest to the obstructed channel (Fig. 3B). In the rear, cells greatly increased in aspect ratio (5.3 ± 2.3) and became highly elongated with very large protrusions, whereas in the front cells were mainly rounded with aspect ratio close to one (1.2 ± 0.2) (p-value < 0.001) (Fig. 3C). We analyzed cell directionality near the obstructed channel and found a bias towards the medium flow (Fig. 3D). Cell directionality in those regions with lower aspect ratio (≈1) was not analyzed, since this parameter is irrelevant in rounded cells. Interestingly we observed the same cellular pattern in the pseudopalisades detected in human GBM samples, with a significant change in the nucleus aspect ratio (2.1 ± 0.5) in the rear end (close to the necrotic core) compared to the front (1.3 ± 0.2) (Fig. 3E and F).

Characterization of pseudopalisade formation

A recent hypothesis about GBM suggests that when migrating cells forming the pseudopalisade reach a new nutrient rich microenvironment (i.e. in the vicinity of a perfused blood vessel) their metabolism changes back to a more proliferative and less migratory state. To test this hypothesis within our system, we analyzed cell proliferation under the different stages of pseudopalisade formation by Ki-67 immunofluorescence. After 5 days under obstructed conditions, we observed no Ki-67 positive cells (Fig. 4A).

On the other hand, when the pseudopalisade was completely formed after 9 days under obstructed conditions, positive cells were observed (Fig. 4B). More interestingly, those proliferative cells appeared only in the vicinities of the perfused microchannel where nutrient concentrations are expected to be highest. Under unrestricted conditions we did not observed positive cells either after 5 or after 9 days (Fig. 4C and D). Central microchamber was vertically divided in three regions and the number of proliferating cell was determined in each one (Fig 4E). The analysis demonstrated most of the proliferating cells were located on the region closest to the perfused lateral microchannel, only a small proportion appeared in the central region, and no proliferating cells were observed in the further region.

To determine if a glucose gradient was generated during long-term experiments, we analyzed the diffusion profile of the fluorescent glucose analog 2-deoxy-2-[(7-nitro-2,1,3-benzoxadiazol-4-yl)amino]-D-glucose (NBDG) across the microchamber in the absence or presence of cells (Supporting Fig. 3) during 2 hours post-NBDG injection. We found little difference in cellular glucose uptake across the microchamber and cells were able to uptake the NBDG. The NBDG diffusion profile without cells (green line) was very similar to the NBDG with cells curve (red line). (Note: the dark areas observed in the assay containing cells are due to light scattering from cells out of the focal plane. Supporting Fig. 4). After removing the NBDG, cell remained labelled in green, showing their ability to incorporate the glucose analog (Supporting Fig. 5). This indicates that during long-term experiments GBM cells are not exposed to a significant glucose gradient and further suggests that pseudopallisading formation is driven by factors other than glucose scarcity.

We next investigated the oxygen profile across the microchamber during experiments using Image-it hypoxia reagent which becomes fluorescent as oxygen tension decreases. Two different sets of experiments were performed, both carried out for 5 days: Under unrestricted conditions medium was pipetted only once a day through both

lateral microchannels. Since both lateral microchannels remained open, the oxygen consumption was symmetric; thereby, a homogeneous hypoxia along the microchamber was generated (Fig 5A and Supporting Fig 6A).

On the other hand, under obstructed conditions the medium flow through the right lateral microchannel guaranteed that oxygen and nutrients in the perfused lateral microchannel were continuously refreshed; whereas the opposed lateral microchannel remained blocked. Thereby, those cells located nearby to the perfused microchannel showed very low hypoxia-induced fluorescence intensity, suggesting a normoxic microenvironment; whereas those cells located nearby the blocked microchannel showed the highest hypoxia-induced fluorescence intensity (Fig 5B, C and Supporting Fig 5B).

These results suggested that gradient conditions were needed to induce the directional migratory process, since under “unrestricted conditions” no directional migration was observed even when a homogenous hypoxia was observed.

Correlation of computer simulations with experimental data

Since the migratory response of the GBM cells is non-linear and not entirely intuitive, we investigated the correlation of our experimental data with simulated computer models. Under unrestricted conditions, the number of cells and their distribution along the chamber vary only slightly due to the very slow proliferation rates we observe (Fig 6A). In our computer simulations, all cells have a normoxic phenotype after 9 days. When the nutrient flow along the left channel was disrupted, cellularity remained spatially homogeneous for 3 days while the nutrient level becomes exhausted, after which cells slowly change their phenotypes. However, our numerical simulations reveal the formation of a pseudopalisade structure moving towards the active channel after 6 days and a dramatic increase in cell density around the flow channel at day 9 (Fig. 6B), which is strongly in agreement with our experiments. Fig. 8C shows the mathematical model scheme used in the computational simulations. We have performed an

extensive parameter value scans and we are forced to conclude that the dynamic behavior observed in our experimental model cannot be reproduced within the framework of the previously published two-phenotype computational model[10,16] which assumes that tumor cells revert to their original normoxic phenotypes when reaching areas of higher oxygenation. Instead, the incorporation of a third highly proliferative phenotype after the wave of migration is essential to reproduce the evolution of our observed cell density profiles during pseudopalisade generation. Our analysis suggests the existence of a highly proliferative GBM cell state triggered by transient waves of metabolic deprivation and migration (Figure 6C).

DISCUSSION

Nutrient and oxygen depletion due to blood vessel obstruction events play an important role on the accelerated spreading of GBM cells across the brain. In this work, we provide a robust and novel methodology to mimic the GBM-associated blood vessel obstruction in vitro. Using our developed microdevice, we were able to culture GBM cells under induced obstructed conditions and for the first time we can demonstrate the formation of a pseudopalisade-like front through several sequential steps. In an initial stage, during the first days under obstructed conditions, there is little morphologic change in the GBM cells as remaining oxygen and nutrients are consumed. In a second stage, nutrient starvation leads to an intense migratory response in those cells located in the starved region, i.e. the pseudopalisade rear. This migratory response creates the observed pseudopalisading structures after six days in culture. Finally, in a third stage, cells of this pseudopalisade front reach the nutrient source (invading the perfused lateral microchannel) and undergo rapid proliferation. This behavior models GBM pseudopalisade progression observed in patients and enables the study of this phenomenon in vitro. The pseudopalisading hypothesis has been suggested to explain the poor improvement on mean survival time achieved by conventional anti-tumorigenic

treatments[21]. Accordingly, the approved chemotherapy treatment for GBM, based on concomitant doses of the alkylating chemotherapy agent temozolomide combined with radiotherapy, only improves mean survival time by a few months compared with radiotherapy only[1,21]. Since most such treatments are focused on killing proliferative cells they do not target those non-proliferative migratory cells of pseudopalisades. Unfortunately, once these cells reach nutrient rich regions they can again become proliferative.

Many recent reports show that cell migration palys a critical role on GBM invasion and spreading, and correlates with patient prognosis[22-24]. In this context, new drugs are being developed to block GBM cells migration[25]. Thus, different animal and in vitro studies show that treatment with specific migration inhibitors can achieve a significantly mean survival time improvement[26,27]. It has been shown GBM cells invade by a mesenchymal migration mode[28-30] based on integrins and matrix degrading enzymes like membrane type matrix metalloproteinase-1 (MT-MMP-1) and MMP-2 [31,32]. These proteins normally are overexpressed in GBM[33]. More interestingly, recent reports have shown hypoxia, through HIF-1α, induce an epithelial-mesenchymal transition (EMT) in GBM cell lines, enhancing cell invasiveness[34]. In our model, cells showed this expected mesenchymal-like GBM migration mode, including the characteristic emission of invadopodia and very large aspect ratio[35]. Our directionality distribution showed that rear cells were preferentially orientated towards the perfused lateral microchannel (the oxygen and nutrient source), forming an angle of 90^{o} with medium flow and aligning in the direction of travel during pseudopalisade formation.

Our oxygen profile measurements reveal that under obstructed conditions cell metabolism creates an oxygen gradient across the microchamber, resembling the hypoxic areas observed in in-vivo pseudopalisades. Our mathematical model suggests the development of a more malignant phenotype after these cycles of hypoxia,

448 migration, and re-oxygenation. This phenotype is highly proliferative and oxygen
449 dependent. Our mathematical simulations support the hypothesis of pseudopalisade
450 formation after a vessel occlusion event and correlate very well with microfluidic device
451 experiments, in which we saw an increase in the cell proliferation when the cells where
452 exposed to obstructed conditions. Our results suggest that both the enhanced
453 infiltration and the malignant phenotype arising after hypoxic cells reach better
454 oxygenated areas may be relevant tumor driving forces originated by microscopic
455 hypoxic events. Therefore, this mathematical model is able to recapitulate the
456 pseudopalisade formation as a hypoxia-driven phenomenon, convincingly reproducing
457 the observed results within the microdevice and the observed pseudopalisades in vivo.
458
459 Our interdisciplinary approach now allows direct observation of GBM invasion and
460 pseudopalisade formation under controlled conditions. Furthermore, the mathematical
461 modeling suggests a sequence of cell states which include alternating phases of
462 hypoxia, invasiveness, and proliferation. These methodologies enable us to see
463 processes once only found in vivo, shed light on the states and life cycle of GBM, and
464 could enable more biologically accurate drug screening methods focused on GBM
465 invasion.
466
467 **ACKNOWLEDGMENTS**

468 The authors thank Dr Mario Durán for all the scientific support and useful discussions.
469 Thanks to José Luis Calavia for his technical support related with the microfluidic
470 system connections and monitoring. This work has been supported by the National
471 Research Program of Spain, projects (dpi2011-28262-c04-01), (MTM2012-31073) and
472 (bes-2012-059940); and Ministerio de Economía y Competitividad/FEDER, Spain
473 [grant number MTM2015-71200-R], Consejería de Educación Cultura y Deporte from
474 Junta de Comunidades de Castilla-La Mancha (Spain) [grant number PEII-2014-031-P]
475 and James S. Mc. Donnell Foundation (USA) 21st Century Science Initiative in

Mathematical and Complex Systems Approaches for Brain Cancer (Special Initiative Collaborative – Planning Grant 220020420 and Collaborative award 220020450). This work was supported by grants from “Ministerio de Economía y Competitividad, Fondo de Investigación Sanitaria” (PI12/00775) to PSG and (PI13/01258) to AHL, and from “Ministerio de Economía y Competitividad, Red Temática de Investigación Cooperativa en Cancer” (RD12/0036/0027) to PSG and AHL. JMA fellowship is provided by the Aragon Government, RM, MVM and GAL fellowships are provided by the Spanish government.

REFERENCES

1. Oike T, Suzuki Y, Sugawara K, et al. Radiotherapy plus concomitant adjuvant temozolomide for glioblastoma: Japanese mono-institutional results. *PloS one.* 2013; 8(11):e78943.

2. Brat DJ. Glioblastoma: biology, genetics, and behavior. *American Society of Clinical Oncology educational book / ASCO. American Society of Clinical Oncology. Meeting.* 2012:102-107.

3. Rong Y, Durden DL, Van Meir EG, Brat DJ. 'Pseudopalisading' necrosis in glioblastoma: a familiar morphologic feature that links vascular pathology, hypoxia, and angiogenesis. *Journal of neuropathology and experimental neurology.* 2006; 65(6):529-539.

4. Brat DJ, Castellano-Sanchez AA, Hunter SB, et al. Pseudopalisades in glioblastoma are hypoxic, express extracellular matrix proteases, and are formed by an actively migrating cell population. *Cancer research.* 2004; 64(3):920-927.

5. Wippold FJ, 2nd, Lammle M, Anatelli F, Lennerz J, Perry A. Neuropathology for the neuroradiologist: palisades and pseudopalisades. *AJNR. American journal of neuroradiology.* 2006; 27(10):2037-2041.

6. Rong Y, Post DE, Pieper RO, Durden DL, Van Meir EG, Brat DJ. PTEN and hypoxia regulate tissue factor expression and plasma coagulation by glioblastoma. *Cancer research.* 2005; 65(4):1406-1413.

7. Brat DJ, Van Meir EG. Vaso-occlusive and prothrombotic mechanisms associated with tumor hypoxia, necrosis, and accelerated growth in glioblastoma. *Laboratory investigation; a journal of technical methods and pathology.* 2004; 84(4):397-405.

8. Jensen RL. Brain tumor hypoxia: tumorigenesis, angiogenesis, imaging, pseudoprogression, and as a therapeutic target. *Journal of neuro-oncology.* 2009; 92(3):317-335.

9. Jain RK, di Tomaso E, Duda DG, Loeffler JS, Sorensen AG, Batchelor TT. Angiogenesis in brain tumours. *Nat Rev Neurosci.* 2007; 8(8):610-622.

10. Martinez-Gonzalez A, Calvo GF, Perez Romasanta LA, Perez-Garcia VM. Hypoxic cell waves around necrotic cores in glioblastoma: a biomathematical model and its therapeutic implications. *Bulletin of mathematical biology.* 2012; 74(12):2875-2896.

11. Bhatia SN, Ingber DE. Microfluidic organs-on-chips. *Nature biotechnology.* 2014; 32(8):760-772.

12. Blanco FJ, Agirregabiria M, Garcia J, et al. Novel three-dimensional embedded SU-8 microchannels fabricated using a low temperature full wafer adhesive bonding. *Micromechanics and Microengineering.* 2004; 14(7):10.

13. Ayuso JM, Monge R, Llamazares G, et al. SU-8 based microdevices to study self-induced chemotaxis in 3D microenvironments. *Front Mater.* 2015; 2: 37(37).

14. Altuna A, Bellistri E, Cid E, et al. SU-8 based microprobes for simultaneous neural depth recording and drug delivery in the brain. *Lab on a chip.* 2013; 13(7):1422-1430.

15. Altuna A, Menendez de la Prida L, Bellistri E, et al. SU-8 based microprobes with integrated planar electrodes for enhanced neural depth recording. *Biosensors & bioelectronics.* 2012; 37(1):1-5.

16. Martinez-Gonzalez A, Duran-Prado M, Calvo GF, Alcain FJ, Perez-Romasanta LA, Perez-Garcia VM. Combined therapies of antithrombotics and antioxidants delay in silico brain tumour progression. *Mathematical medicine and biology : a journal of the IMA.* 2014.

17. Hatzikirou H, Basanta D, Simon M, Schaller K, Deutsch A. 'Go or grow': the key to the emergence of invasion in tumour progression? *Mathematical medicine and biology : a journal of the IMA.* 2012; 29(1):49-65.

18. Jeong GS, Han S, Shin Y, et al. Sprouting angiogenesis under a chemical gradient regulated by interactions with an endothelial monolayer in a microfluidic platform. *Analytical chemistry.* 2011; 83(22):8454-8459.

19. Kim C, Kasuya J, Jeon J, Chung S, Kamm RD. A quantitative microfluidic angiogenesis screen for studying anti-angiogenic therapeutic drugs. *Lab on a chip.* 2015; 15(1):301-310.

20. Kothapalli CR, van Veen E, de Valence S, et al. A high-throughput microfluidic assay to study neurite response to growth factor gradients. *Lab on a chip.* 2011; 11(3):497-507.

21. Peponi E, Tourkantonis I, Tasiou I, Pavlidis N, Pentheroudakis G, Tsekeris P. Prognostic factors in glioblastoma patients managed with radiotherapy combined with temozolomide. *Journal of B.U.ON. : official journal of the Balkan Union of Oncology.* 2014; 19(3):718-723.

22. Vehlow A, Cordes N. Invasion as target for therapy of glioblastoma multiforme. *Biochimica et biophysica acta.* 2013; 1836(2):236-244.

23. Moller HG, Rasmussen AP, Andersen HH, Johnsen KB, Henriksen M, Duroux M. A systematic review of microRNA in glioblastoma multiforme: micro-modulators in the mesenchymal mode of migration and invasion. *Mol Neurobiol.* 2013; 47(1):131-144.

24. Lefranc F, Brotchi J, Kiss R. Possible future issues in the treatment of glioblastomas: special emphasis on cell migration and the resistance of migrating glioblastoma cells to apoptosis. *Journal of clinical oncology : official journal of the American Society of Clinical Oncology.* 2005; 23(10):2411-2422.

557 **25.** Scaringi C, Minniti G, Caporello P, Enrici RM. Integrin inhibitor cilengitide for the
558 treatment of glioblastoma: a brief overview of current clinical results. *Anticancer*
559 *research.* 2012; 32(10):4213-4223.
560 **26.** Munson JM, Fried L, Rowson SA, et al. Anti-invasive adjuvant therapy with imipramine
561 blue enhances chemotherapeutic efficacy against glioma. *Science translational*
562 *medicine.* 2012; 4(127):127ra136.
563 **27.** Zhang L, Wang H, Zhu J, Ding K, Xu J. FTY720 reduces migration and invasion of human
564 glioblastoma cell lines via inhibiting the PI3K/AKT/mTOR/p70S6K signaling pathway.
565 *Tumour biology : the journal of the International Society for Oncodevelopmental*
566 *Biology and Medicine.* 2014.
567 **28.** Myung JK, Choi SA, Kim SK, Wang KC, Park SH. Snail plays an oncogenic role in
568 glioblastoma by promoting epithelial mesenchymal transition. *International journal of*
569 *clinical and experimental pathology.* 2014; 7(5):1977-1987.
570 **29.** Piao Y, Liang J, Holmes L, Henry V, Sulman E, de Groot JF. Acquired resistance to anti-
571 VEGF therapy in glioblastoma is associated with a mesenchymal transition. *Clinical*
572 *cancer research : an official journal of the American Association for Cancer Research.*
573 2013; 19(16):4392-4403.
574 **30.** Caspani EM, Echevarria D, Rottner K, Small JV. Live imaging of glioblastoma cells in
575 brain tissue shows requirement of actin bundles for migration. *Neuron Glia Biol.* 2006;
576 2(2):105-114.
577 **31.** Hotary K, Allen E, Punturieri A, Yana I, Weiss SJ. Regulation of cell invasion and
578 morphogenesis in a three-dimensional type I collagen matrix by membrane-type
579 matrix metalloproteinases 1, 2, and 3. *The Journal of cell biology.* 2000; 149(6):1309-
580 1323.
581 **32.** Friedl P. Prespecification and plasticity: shifting mechanisms of cell migration. *Current*
582 *opinion in cell biology.* 2004; 16(1):14-23.

583 **33.** Yamamoto M, Ueno Y, Hayashi S, Fukushima T. The role of proteolysis in tumor
584 invasiveness in glioblastoma and metastatic brain tumors. *Anticancer research.* 2002;
585 22(6C):4265-4268.
586 **34.** Joseph JV, Conroy S, Pavlov K, et al. Hypoxia enhances migration and invasion in
587 glioblastoma by promoting a mesenchymal shift mediated by the HIF1alpha-ZEB1 axis.
588 *Cancer letters.* 2015.
589 **35.** Yilmaz M, Christofori G, Lehembre F. Distinct mechanisms of tumor invasion and
590 metastasis. *Trends in molecular medicine.* 2007; 13(12):535-541.

591

592

593

Fig 1. Experimental set-up. A) Scheme of pseudopalisade formation. Under obstructed conditions, nutrient scarcity triggers a migratory response in those cells located in the obstructed blood vessel vicinity (I) towards enriched regions (II). B) Experimental scheme within the microdevice, mimicking the obstructed conditions and the starved (I) and enriched (II) region. C) Fabricated microdevice and packaging tool. D) Microfluidic system. E) U-251 cell viability within the microdevice after 9 days, live cells (labelled with Calcein 1 μg/ml) are shown in green whereas dead cells are in red (labelled with Propidium iodide 4 μg/ml). Microdevice posts (50x100 μm) are delimited in white dashed line. Cells were cultured at 4 million cells/ml within a 1.5 mg/ml collagen hydrogel. Viable cells are shown in green, whereas dead ones are in red. F) Cell viability comparison between hydrogels on Petri dishes (red) and within the microdevice (blue). Cell viability is expressed as the percentage of live cells. Scale bar is 200 μm.

Fig 2. Pseudopalisade formation under obstructed conditions. U-251 at 4 million cells/ml in collagen hydrogel at 1.5 mg/ml were culture within microdevices. Under unrestricted conditions medium was refreshed once a day and cell viability was evaluated at three (A), six (B) and nine (C) days using Calcein (green) and propidium iodide (red). To mimic obstructed conditions, medium flow was enabled only through right microchannel and cell viability was assessed at three (D), six (E) and nine (F) days. Microdevice posts (50x100 μm) are delimited in white dashed line. Graphs show the fluorescence intensity across the microchamber orthogonal view at three (G), six

(H) and nine days (I) in obstructed as unrestricted conditions. Post position in the graphs is delimited by gray dashed line. Scale bar is 200 µm.

Fig 3. Cell shape during Pseudopalisade formation. Confocal images of the microchamber after five days in culture under unrestricted (A) or obstructed conditions were taken (B). C) Cell shape at the pseudopalisade rear and front was analyzed and compared with the same region under unrestricted conditions, *** denotes a statistical difference (p-value $1.4x10^{-32}$). D) Directionality at the pseudopalisade rear under obstructed conditions. E) H&E staining of a paraffin-embedded GBM sample. F) Nucleus aspect ratio in the pseudopalisade rear and front in patient samples, *** denotes a statistical difference (p-value $3.7x10^{-8}$). Scale bar is 200 µm.

Fig 4. Proliferation during pseudopalisade formation. Ki-67 immunofluorescence was performed within the microdevices during the different steps of the pseudopalisade formation. A-B) Under obstructed conditions, ki-67 positive cells were observed only after 9 days, when the pseudopalisade was completely formed. C-D) Under unrestricted conditions no positive cells were observed at 5 or 9 days. Scale bar is 200 µm.

Fig 5. Oxygen profile. Oxygen profile was detected after 5 days in culture using Image-it Hypoxia reagent and images are shown as heat-map hypoxia-induced fluorescence intensity. Hypoxia-induced fluorescence intensity across the microchamber revealed oxygen concentration was constant under unrestricted conditions (A), whereas under obstructed conditions an oxygen gradient was established (B). The graph shows the hypoxia-induced fluorescence intensity profile across the microchamber (C). Scale bar is 200 µm.

Fig 6. Computer simulations versus experimental data of the cell evolution profiles. Simulations of tumor cell density evolution and experimental data of fluorescence intensity within the chamber under unrestricted conditions (A) and under

obstructed conditions (B). Left Y axis denotes fluorescence intensity from experiments at day 3, 6 and 9, curves red blue and black respectively. Right Y axis denotes cell density from simulations at day 3, 6 and 9, red spots, blue cross and black circles respectively. Post position in the graphs is delimited by gray dashed line. C) Graphical depiction of the mathematical model scheme based on previous models [10, 13] and including three cancer cell phenotypes, the oxygenation and the necrosis (C).

Fig 1.

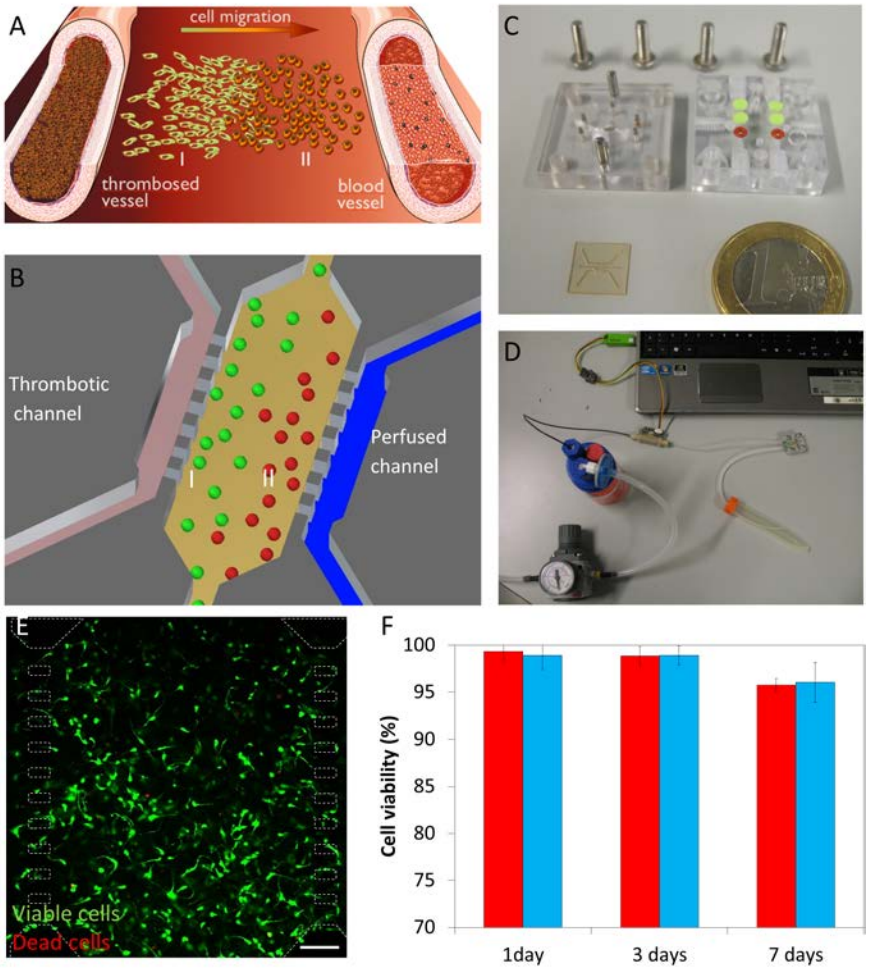
A
cell migration
I
II
thrombosed vessel
blood vessel
B
Thrombotic channel
Perfused channel
I
II
C
D
E
Viable cells
Dead cells
F
Cell viability (%)
100
95
90
85
80
75
70
1day
3 days
7 days

Fig 2.

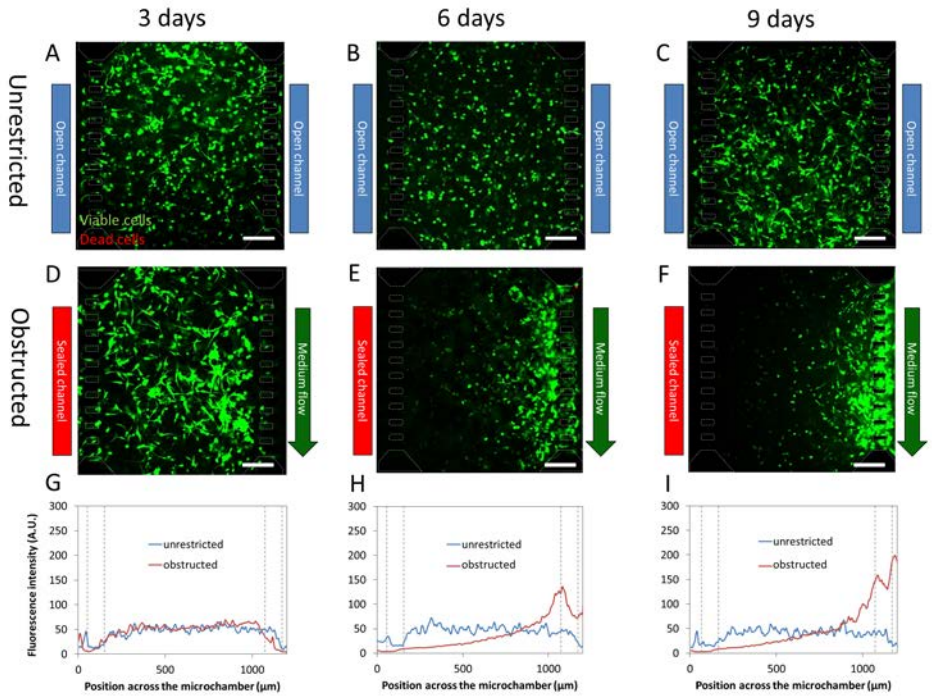
3 days
6 days
9 days
A
B
C
Unrestricted
Open channel
Open channel
Viable cells
Dead cells
D
E
F
Obstructed
Sealed channel
Medium flow
G
H
I
Fluorescence intensity (A.U.)
unrestricted
obstructed
Position across the microchamber (μm)

658 **Fig 3.**

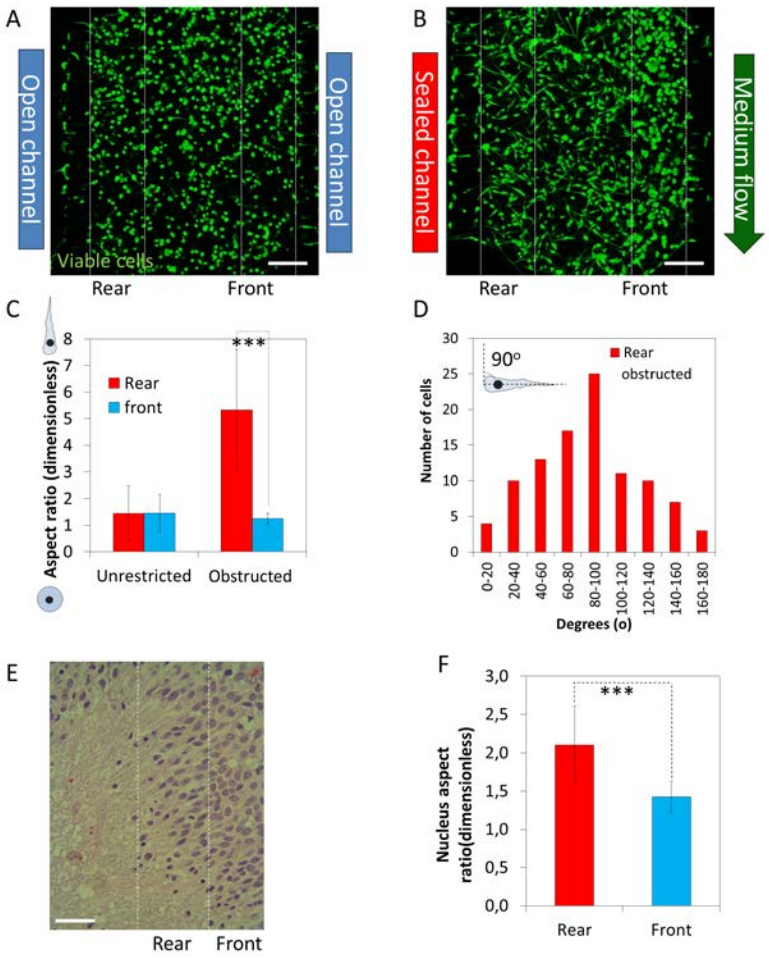

659

660

Fig 4.

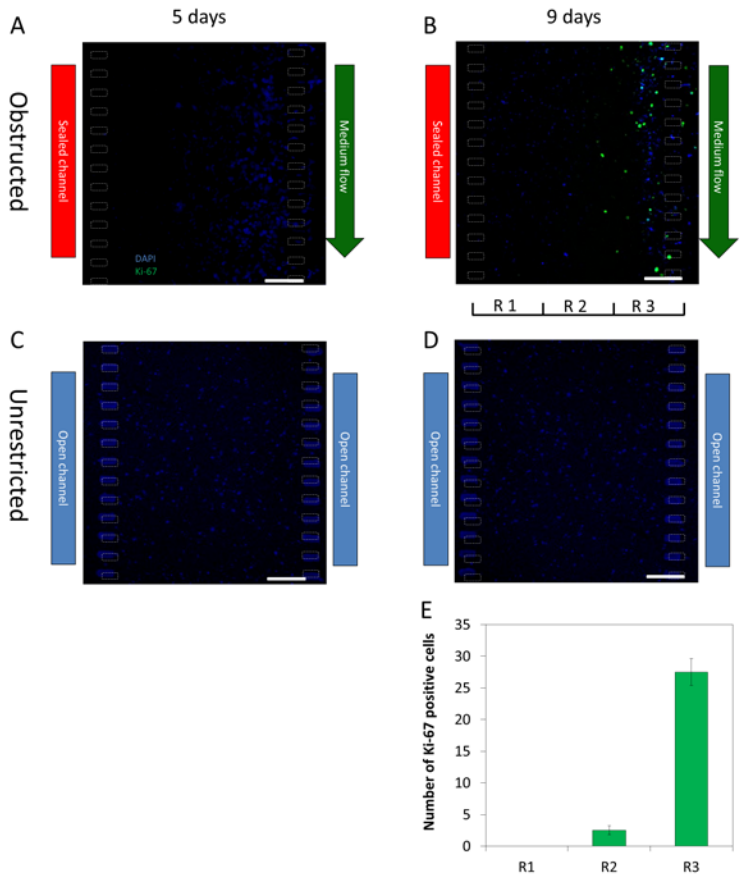
A
5 days
Obstructed
Sealed channel
Medium flow
DAPI
Ki-67
B
9 days
Sealed channel
Medium flow
R 1
R 2
R 3
C
Unrestricted
Open channel
Open channel
D
Open channel
Open channel
E
Number of Ki-67 positive cells
35
30
25
20
15
10
5
0
R1
R2
R3

Fig 5.

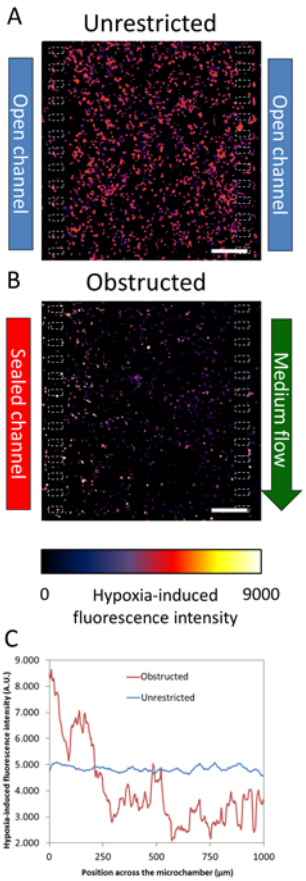
A
Unrestricted
Open channel
Open channel
B
Obstructed
Sealed channel
Medium flow
0
Hypoxia-induced
fluorescence intensity
9000
C
Obstructed
Unrestricted
Hypoxia-induced fluorescence intensity (A.U.)
9.000
8.000
7.000
6.000
5.000
4.000
3.000
2.000
0
250
500
750
1000
Position across the microchamber (µm)

672 **Fig 6.**

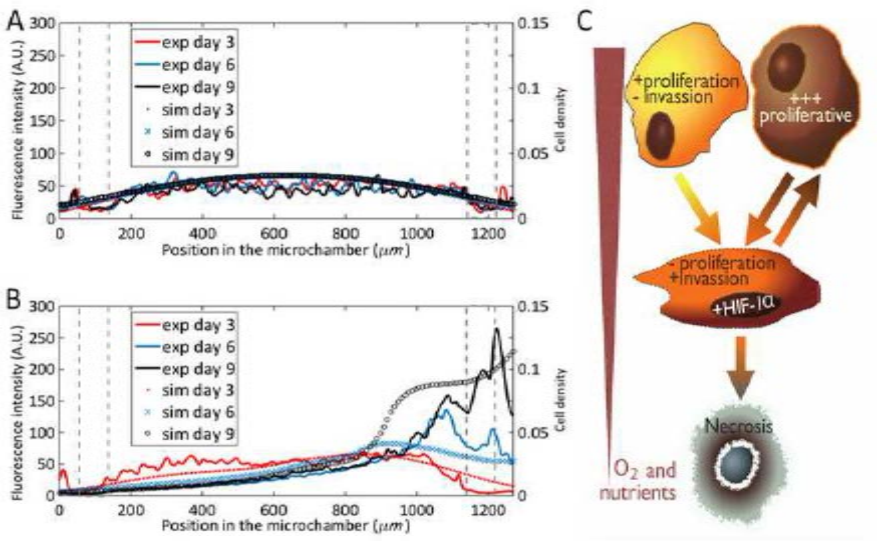

673

674

Supporting Fig 1. Flow characterization. Green-fluorescent spheres were dissolved in the culture medium to study the flow profile during long-term experiments under obstructed conditions. A-C) Fluorescent time-lapse images during obstructed conditions showed no sphere penetration in the hydrogel. D-F) Interstitial flow through the hydrogel was created opening one of the inlets of the “sealed” lateral microchannel and closing one of the “perfused” one to illustrate the fluorescent spheres penetration. Scale bar is 200 µm.

Supporting Fig 2. C6 cells cultured within the microdevices. 4 million C6 GBM cells/ml were embedded in a 1.2 mg/ml collagen hydrogel and confined in the central microchamber. Microdevices were cultured under unrestricted conditions (A) or obstructed conditions (B). After 3 days, cell viability was analyzed with CAM/PI staining; showing viable cells in green and dead ones in red. Graphs show the viable/dead cell fluorescence intensity distribution along the delimited region (yellow rectangle in the images). Pillar position is shown in dashed line. Scale bar is 200 µm.

Supporting Fig 3. Glucose profile. Glucose-free culture medium supplemented with 200 µm NBDG was perfused through the lateral microchannel. Cells were fluorescently labelled in red and the NBDG diffusion profile was studied in the presence (red line) and absence (green line) of cells after 10 (A), 60 (B) and 120 (C) min. Scale bar is 200 µm.

Supporting Fig 4. NBDG diffusion profile. During NBDG diffusion, dark spots were observed within the hydrogel when DiI-labelled cells were present. Those spots corresponded to cells out of focus that caused green-light scattering. Scale bar is 200 µm.

Supporting Fig 5. NBDG uptake. After perfusing NBDG through the right microchannel, growth medium was perfused through the system to remove the NBDG. DiI-labelled cells remained fluorescent in the hydrogel, and now green fluorescent was

observed within the cells, demonstrating their ability to incorporate the NBDG. Scale bar is 200 µm.

Supporting Fig 6. Oxygen profile. Oxygen profile was detected after 5 days in culture using Image-it Hypoxia reagent. Hypoxia-induced fluorescence intensity across the microchamber revealed oxygen concentration was constant under unrestricted conditions (A), whereas under obstructed conditions an oxygen gradient was established (B). Scale bar is 200 µm.

709 **Supporting Fig 1.**

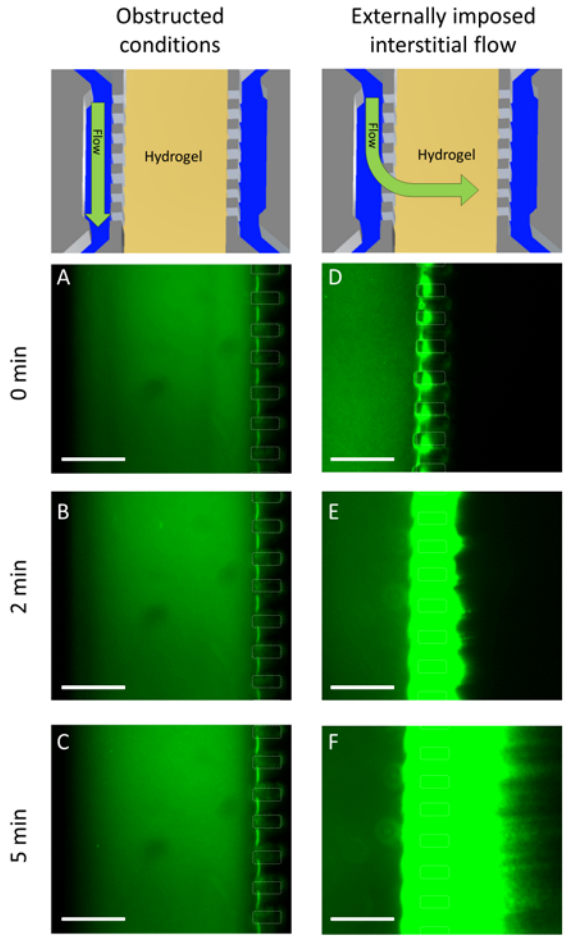

710

711

712 **Supporting Fig 2.**

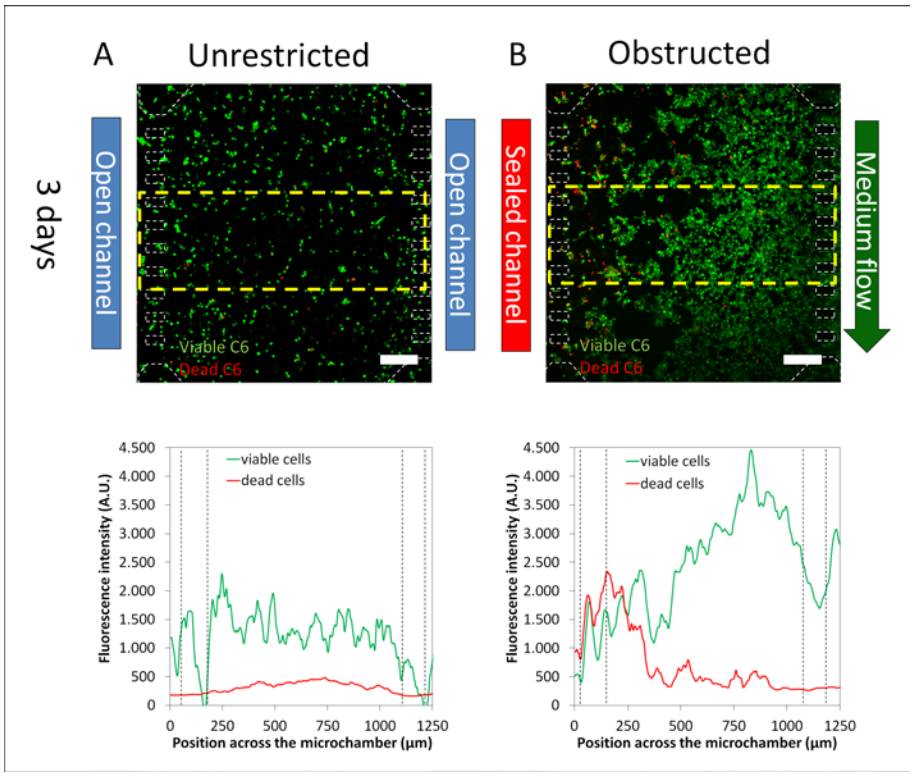

713

714

Supporting Fig 3.

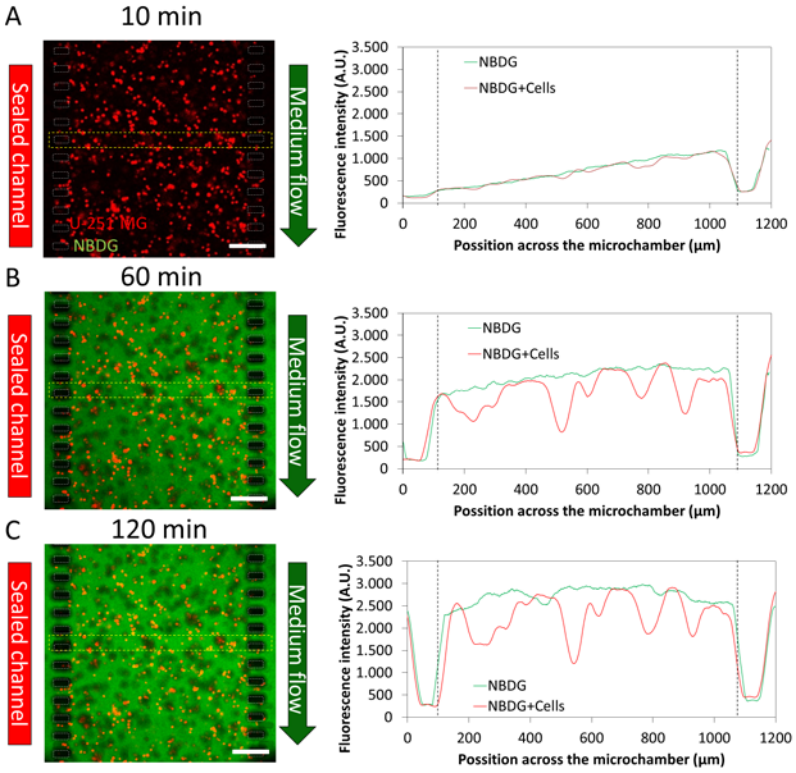

719 **Supporting Fig 4.**

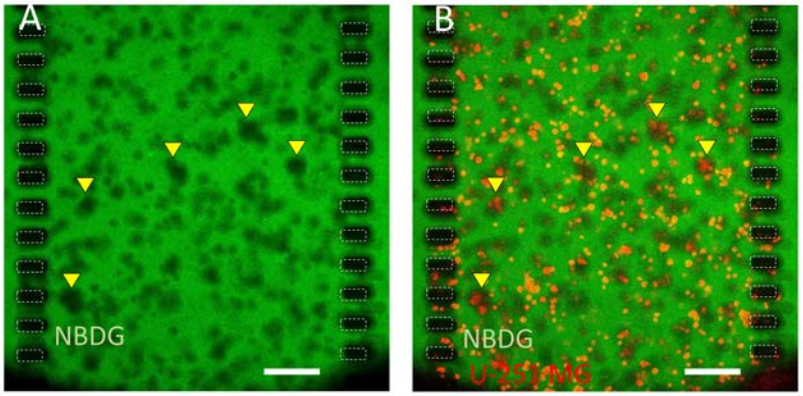

720

721

722 **Supporting Fig 5.**

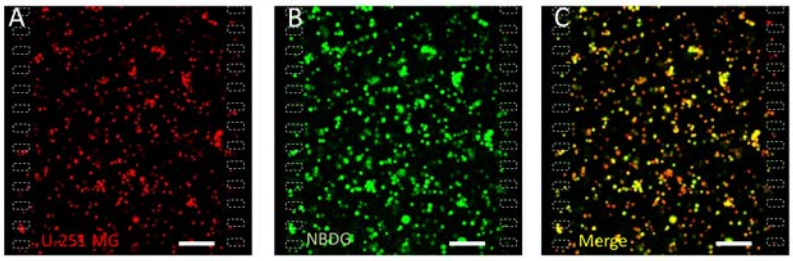

723

724

725

726 **Supporting Fig 6.**

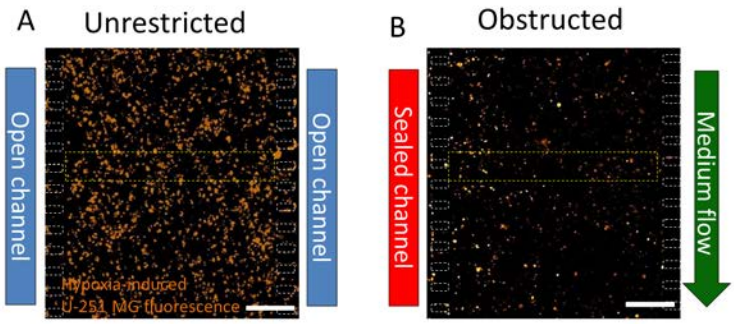

727